CNRS
Centre National de la Recherche Scientifique

INFN
Istituto Nazionale di Fisica Nucleare

Auxiliary Laser system: fibre phase noise measurement and cavity lock requirements

VIR-0540A-16

Julia Casanueva[1*], Gabriel Pillant[2], Eric Genin[2], and Nicolas Leroy[1]

[1] *LAL - Laboratoire de l'Accelerateur Lineaire*
[2] *EGO - European Gravitational Observatory*

Date: December 20, 2016

[*] *corresponding author:* casanuev@lal.in2p3.fr

VIRGO* A joint CNRS-INFN Project
Via E. Amaldi, I-56021 S. Stefano a Macerata - Cascina (Pisa)
Secretariat: Telephone (39) 050 752 521 * FAX (39) 050 752 550 * Email: ego@ego-gw.it

Contents

1 Introduction

The lock strategy of the Signal Recycled Interferometer is based on the use of Auxiliary lasers with a different wavelength than the carrier, for which the arm cavities have a lower finesse. The wavelength has been chosen to be 532 nm in order to be easily compared with the main laser [1]. In the schema used at LIGO this green beam is injected from the end station and subsequently locked to the cavity. Once this is done, the transmission is recovered at the central part and used to extract information about the differential and common modes that will be used for the global lock strategy [2].
However, the laser beam at the end station has to be stable enough to lock the cavities and it also has to be related to the main laser so that the lock hand-off from the auxiliary laser to the main one can be done in a controlled way. For both purposes it is necessary to bring a part of the main laser to the end station to be used as reference. The intention is to re-use already installed Telecom optical fibres, and the aim of the work presented here is to figure out how the propagation through 3 km of fibre affects the beam in terms of phase noise and polarization to determine whether a noise cancellation system and/or a power stabilisation will be needed.

2 Experimental setup and measurements

In order to measure the noise introduced by the fibre, a 1064 nm laser (P_{in} = 100 mW) is split in two beams: one that is used as reference (20% of the input power), and another one that is shifted in frequency (@ 80 MHz) and injected into a fibre (80% of the input power). The interference of both beams provides information about the phase difference between them, meaning the extra noise added by the fibre. The experimental setup used is shown in Figure 1.

Notice that at the exit of the fibre there is a polarizing cube to ensure the interference with the reference

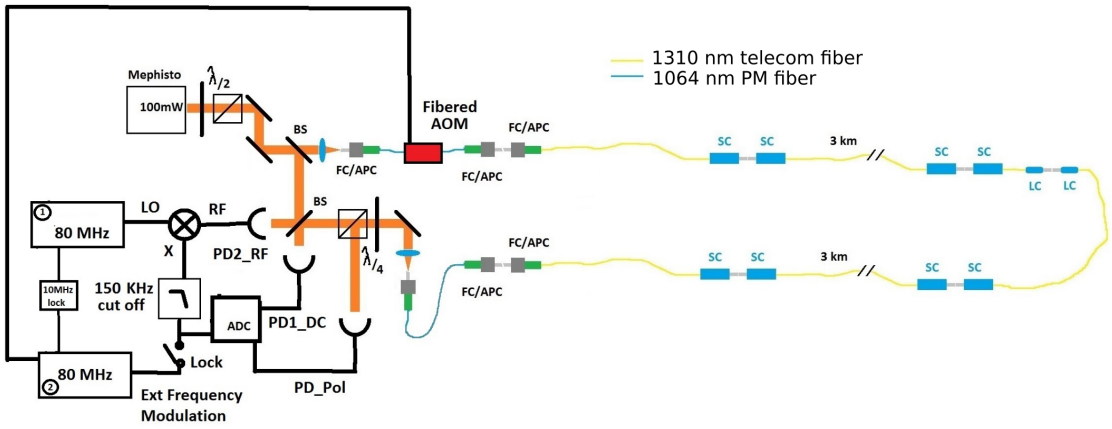

Figure 1: Scheme of the experimental setup

beam. It also allows to monitor the fluctuation of the polarization due to the passage through the fibre by adding a photodiode (PD_Pol) as shown in Figure 1. The interference is monitored by two photodiodes: one that measures the DC (PD1_DC) and another one that is demodulated (PD2_RF) and low pass filtered. It is this signal which contains the phase noise.

We made two types of measurements depending on the demodulation of PD2_RF:

- The demodulation is done at $f_{mod} + \delta$f [3] and so all the information about the phase noise will be around δf (A·cos($\delta\omega$ ·t - ϕ(t))).

- The demodulation is done at f_{mod} and so the beat note gives us information about the phase noise (A·cos(ϕ(t))). With this measurement, we can filter the signal and send it back to the AOM as a correction, locking the fibred arm to the reference one. It will give us an experimental confirmation that the noise could be reduced if necessary.

We also tested two lengths of fibre:

- A 1064 nm PM fibre of 20 m, where we are sure that our laser is coherent.
- A 6 km 1319 nm Telecom fibre already installed between the central and the arms buildings, which we are interested in testing because it will be the one that we intend to use in the final design to propagate a part of the main laser. Notice that the coherence of our laser is >1 km so it will have an impact on this measurement.

3 Results

3.1 Measurement with a 20m fibre

First of all we made a measurement of the detection noise limit by using the setup shown in Figure 1 without the long fibre (this means only 1 m of fibre). We used the first method described before, demodulating at 80 MHz + 3344.5 Hz. The blue curve on Figure 2 shows the result of this measurement. It can be seen that the FWHM is smaller than 0.1 Hz

After we made a first measurement of the phase noise by using 20m of fibre rolled up inside a box where we could add perturbations (acoustic and thermal). Using the same demodulation frequency as for the previous measurement, the result is shown in Figure 2, the black line.
It can be seen that there is a broadening on the linewidth of the laser due to the phase noise introduced on

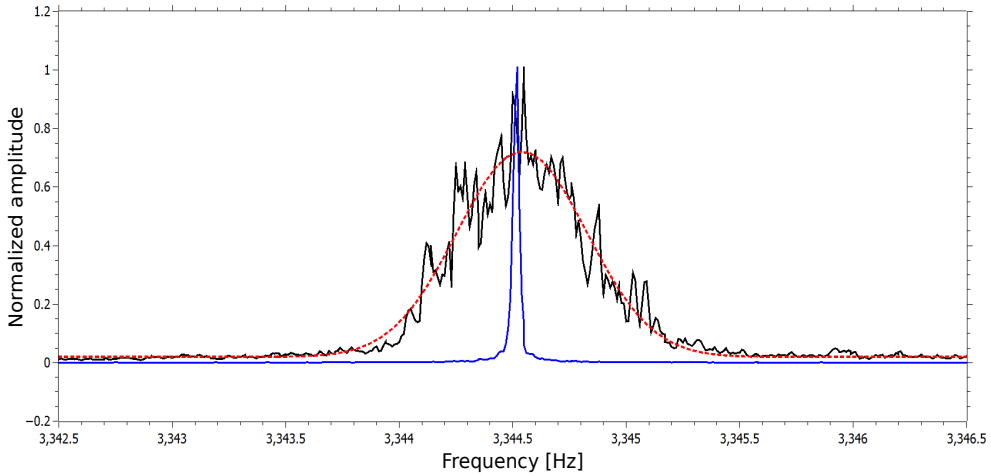

Figure 2: The blue curve shows the detection limit of our setup, with a FWHM of less than 0.1 Hz. The black curve shows a measure of the phase noise introduced by a fibre of 20 m. The FWHM is lower than 1 Hz. Both measurements have been taken by demodulating the interference at 80 MHz + 3344.5 Hz.

the 20 m of fibre. The spectrum can be fitted to a gaussian with a FWHM below 1 Hz.

3.2 Measurement with a 6km fibre

For this measurement, we moved the breadboard used for the 20 m test to the DAQ room [5], in order to inject the laser beam into the fibres that we are interested in testing. First of all we checked that the power loss after passing through the 6 km of fibre agrees with what expected from the fused silica absorption coefficient, 1 dB/km (1/4 of the input power in total). However, the throughput power is in any case limited by the stimulated Brillouin scattering (SBS) [6].

Regarding the polarization of the beam at the output of the fibre we looked at the power arriving to the photodiode PD_Pol (see Figure 1), which monitors the power on the P polarization and the photodiode PD1_DC which monitors half of the power on the S polarization. Figure 3 shows the power on the S polarization during 10 hours, and its statistical distribution.

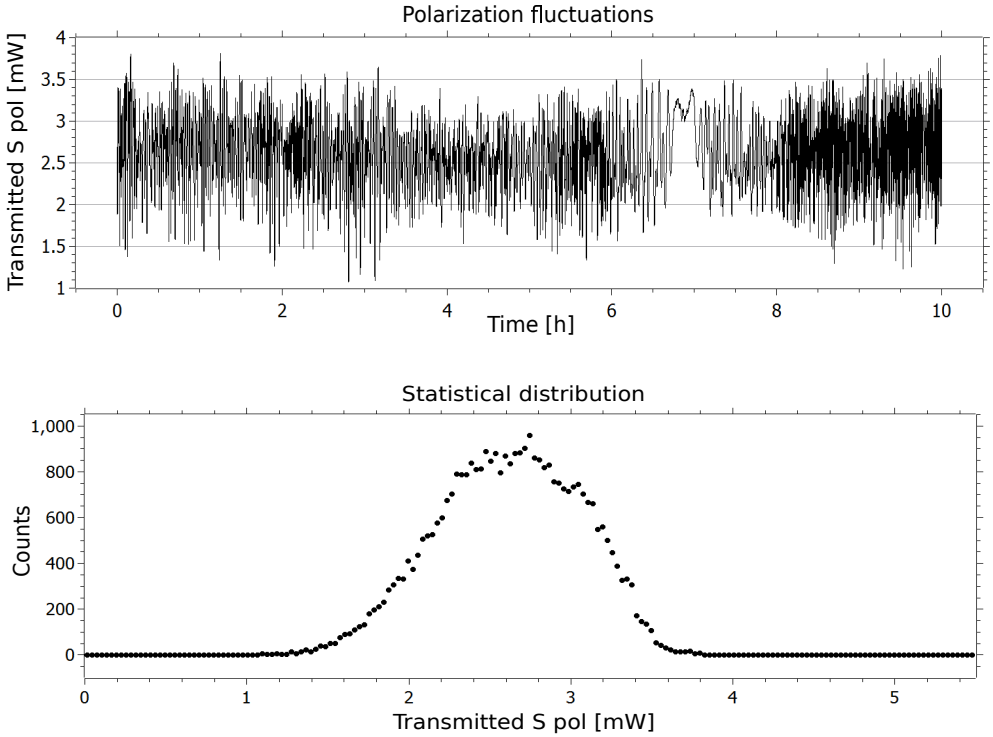

Figure 3: **Upper figure:** Power on the S polarization at the output of the fibre during a period of time of 10 hours. **Lower figure:** Statistical distribution of the power on the S polarization at the output of the fibre during the same period of time

Notice that the power never extinguishes, and so that both polarizations P and S are always present. This means that the fibre has a depolarizing effect [7], and in practice we can see on Figure 3 that the power carried by the S polarization never goes under 1 mW. As a consequence, a power stabilisation will be needed at the exit of the fibre.

The different measurements done on the phase noise added by the fibre are shown in Figure 4. The black line is the spectrum of the signal obtained when demodulating at 80 MHz. The beige line corresponds to the spectrum when we are locked. Finally the violet line is the spectrum when demodulating at 80 MHz + 4100 Hz.
Notice that we are still able to lock after 6 km of fibre. Figure 5 shows the beat note obtained while demodu-

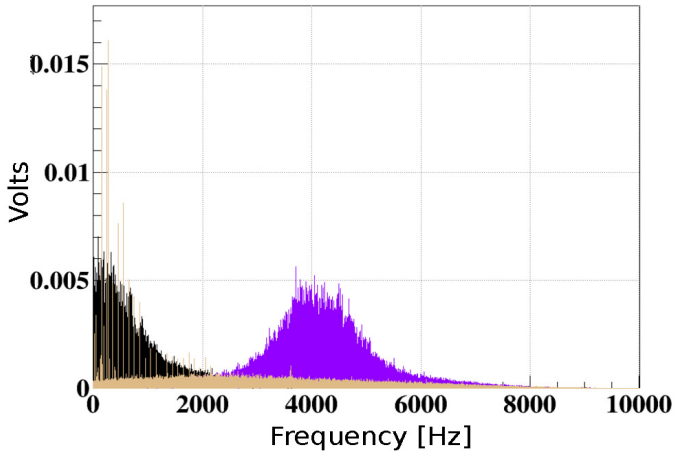

Figure 4: FFT of the signal obtained from the PD2_RF. The black line is the signal when demodulated at 80 MHz, the beige line is the signal when locked, and the violet signal is the one when demodulated at 80 MHz + 4100 Hz

lating at 80 MHz (black) and the one obtained during lock (violet).

As mentioned before, in this configuration we can not be sure if the lasers are fully coherent when interfering

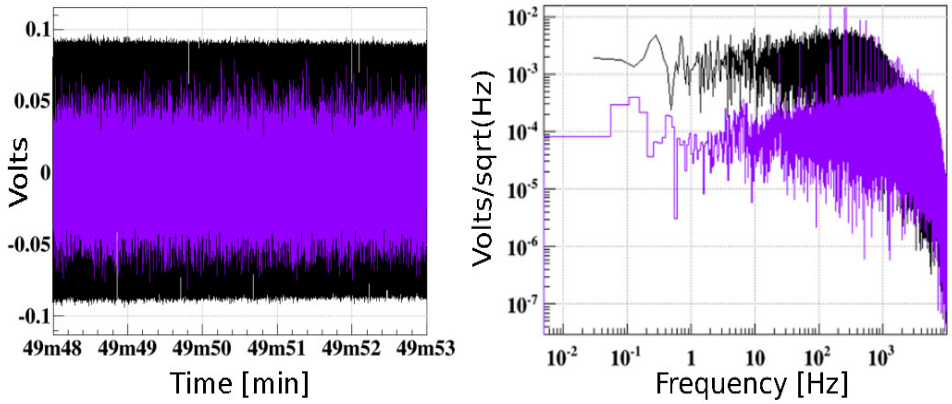

Figure 5: PD2_RF temporal signal (Upper picture) and its FFT when demodulated at 80 MHz (black) and when locked (violet) (Lower picture).

(coherence > 1 km) and so this time the beat note will give us information about the phase noise and the frequency fluctuations of the laser itself. Figure 6 shows the fit of spectrum at 80 MHz + 4100 Hz. The beat note is the convolution of the distribution of both interfering beams. It can be seen that the data fit is closer to a Lorentzian (with a FWHM of 1.47kHz) [4] than to a Gaussian. This indicates that we are dominated by the laser frequency fluctuations, since we expect a gaussian distribution from the phase noise, as seen in Figure 2. Knowing that the convolution of two Lorentzian distributions with a given FWHM is a Lorentzian with twice that FWHM [15], and assuming that the induced phase noise is proportional to the fibre length, we can say that for a fibre of 3 km the expected broadening of the laser linewidth is at most ∼740 Hz. Notice that the central frequency is the one of the main laser while locked to the reference cavity.

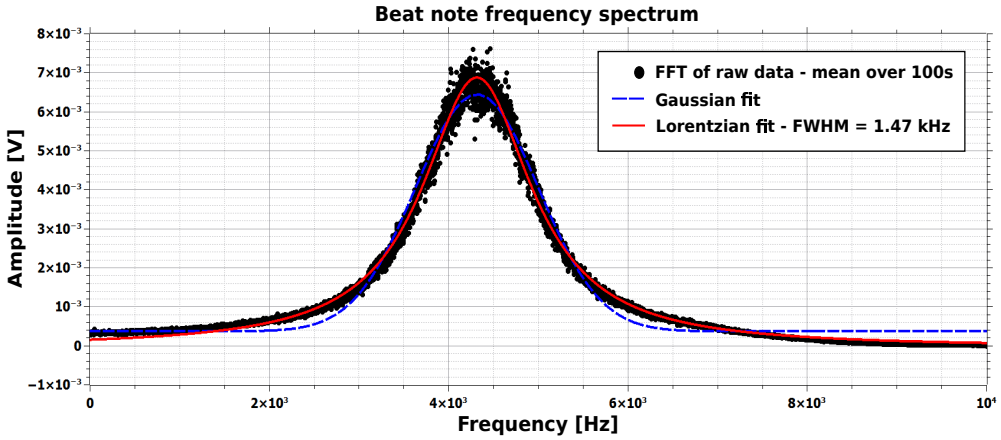

Figure 6: Fit to the FFT of the PD2_RF signal when demodulating at 80 MHz + 4100 Hz.

4 Lock requirements and simulation

As explained in the introduction, one of the aims of this measurement is to determine whether the extra phase noise due to the passage through the fibre will prevent the lock of the arm cavities. A study of the system from the control point of view is needed for this purpose. The performance of a lock can be evaluated by the **residual frequency variation** of the laser once the control is engaged. The requirements on this variation depend on the target pursued. For the control of Advanced Virgo in Science Mode the requirements are based on the power fluctuations that are acceptable, and they were fixed at 10^{-3}, which is one order of magnitude lower than the ones for Virgo (10^{-2}) [8]. However, our aim is not to reach the maximum sensitivity but to keep the arms out of a resonance of the main laser(1064 nm). For this reason the requirements for the Auxiliary Laser control can be relaxed to purely lock acquisition considerations. A safe limit has been set to 10^{-1} power fluctuations, which for a finesse of 190 means a RMS frequency variation of 40Hz. Notice that both arms have not the same finesse for the green light (150 and 190 according to the measurements done by LMA [9] [10] [11] [12]) and so the study has been done for the highest, for being the worst case scenario.

4.1 Control system overview

A standard feedback system is composed of several elements. The main one is the **plant**, which is the element to be controlled. In our case is a Fabry-Perot cavity which needs to be kept in resonance. After, an **error signal** is necessary in order to have information about how far is the system from the working point. The PDH technique is used for this purpose, in particular an AOM has been chosen as modulator because it acts on the frequency of the laser. The error signal is then sent to a **filter** that calculates the correction needed to bring the cavity back to resonance. Finally this correction is sent to the **actuator** which adjusts the system consequently.

There are two possibilities at the level of the actuation: *to act on the mirror* to correct the cavity length or *to act on the laser* to correct its frequency. The main difference between both is the control bandwidth that can be achieved. The bandwidth of a mechanical lock is usually low (hundreds of Hz). In Virgo it is limited by the delay due to communication between different elements. However, another limiting factor is the transfer function of the mirror mechanics which attenuates the frequencies over its resonance (0.8 Hz). This means that in order to act at high frequencies a lot of correction would be needed, reaching the limit of the actuator dynamics. This control at low frequencies is enough for suppressing the seismic noise but not the frequency noise, which is still important at high frequencies.
Traditionally in Virgo the lock acquisition of the arm cavities is done by acting on the mirror position because

the laser frequency is pre-stabilized thanks to the Input Mode Cleaner and the Reference Cavity and so it does not contribute to the noise at high frequencies. Nevertheless, since we are concerned about the frequency noise after the fibre, a high control bandwidth will be needed. This is the reason why an actuation on the laser frequency is planned. This type of actuation rises the control bandwidth specially when used analogically, because the delay can be reduced significantly and the response of the actuation is flat, avoiding saturation of the dynamics.
In our case a VCO has been chosen as actuator. Its aim is to change the frequency of its output sine depending on the input voltage. This sine drives the frequency of the acoustic wave generated on the AOM, shifting the frequency of the laser and bringing the system back to resonance.

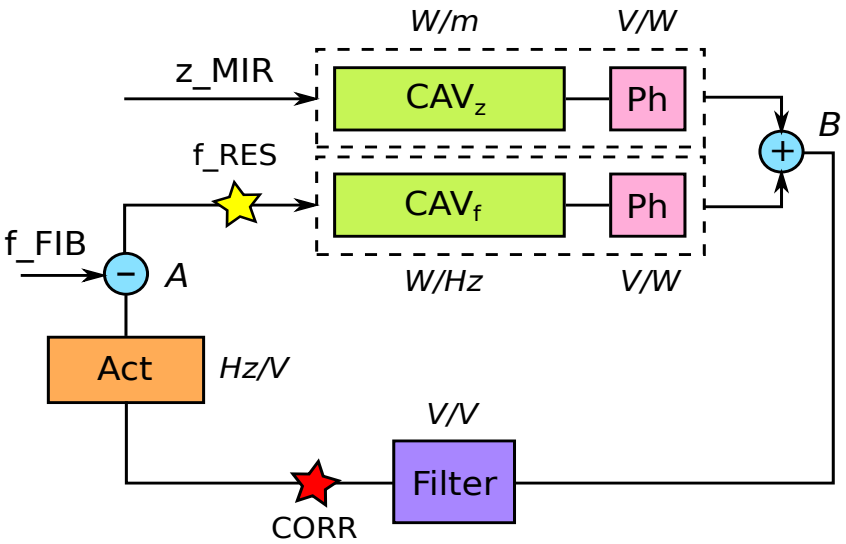

Figure 7: Schema of the control system. The boxes represent the Transfer Function of the different elements. There are two inputs that correspond to the noises that perturb the system. The two stars represent the points that need to be studied in order to determine the loop performance.

Figure 7 shows the scheme of the control system that has been foreseen. The green boxes represent the cavity transfer functions. That is the response of the cavity (in Watts) to a variation of its length (CAV_z) or to a variation of the laser frequency (CAV_f). The error signal is acquired by a photodiode, which is represented by the pink boxes. Its transfer function is flat up to the MHz range. For a matter of simplicity we have considered them as transparent because they only contribute with a calibration factor which does not change the performance of the control loop. The control filter is represented by a purple box and its response in Volts is sent to the orange box which corresponds to the actuator transfer function. Their shapes are described in the next section.

4.2 Open Loop and control filter

The key part of the control loop is the filter. It needs to be designed taking in account the behaviour of the rest of the elements of the system in order to assure the overall stability. The first step is to know the Open Loop transfer function of the system we want to study. It describes the functioning of the system when the control is not engaged. It is the equivalent of disconnecting the exit of the actuator from the summation point A in Figure 7. Its expression is written as:

$$OL_{Las} = CAV_f \cdot Filter \cdot Act \tag{4.1}$$

The transfer functions (TFs) of the cavity (both as a function of the laser frequency and as a function of the cavity length) have been simulated with Finesse [13]. They are characterized by a simple pole at a frequency, f_p, which is equal to half the linewidth of the resonance. In this case f_p is at ∼131.6 Hz. Figure 8 shows both TFs, which are identical below the pole except for the calibration factor (one is in W/m and the other in W/Hz).

Around the Free Spectral Range there is a peak on the CAV_z TF and a notch on the CAV_f TF. This behaviour is relevant because at this frequency (FSR 50KHz) the Transfer Function of the cavity suffers a phase change of 360°, which can not be compensated with the filter and which will make the system unstable [14]. It is particularly delicate because it will not appear on the stability diagram, causing confusion about its real impact. This behaviour is shown in Figure 8.

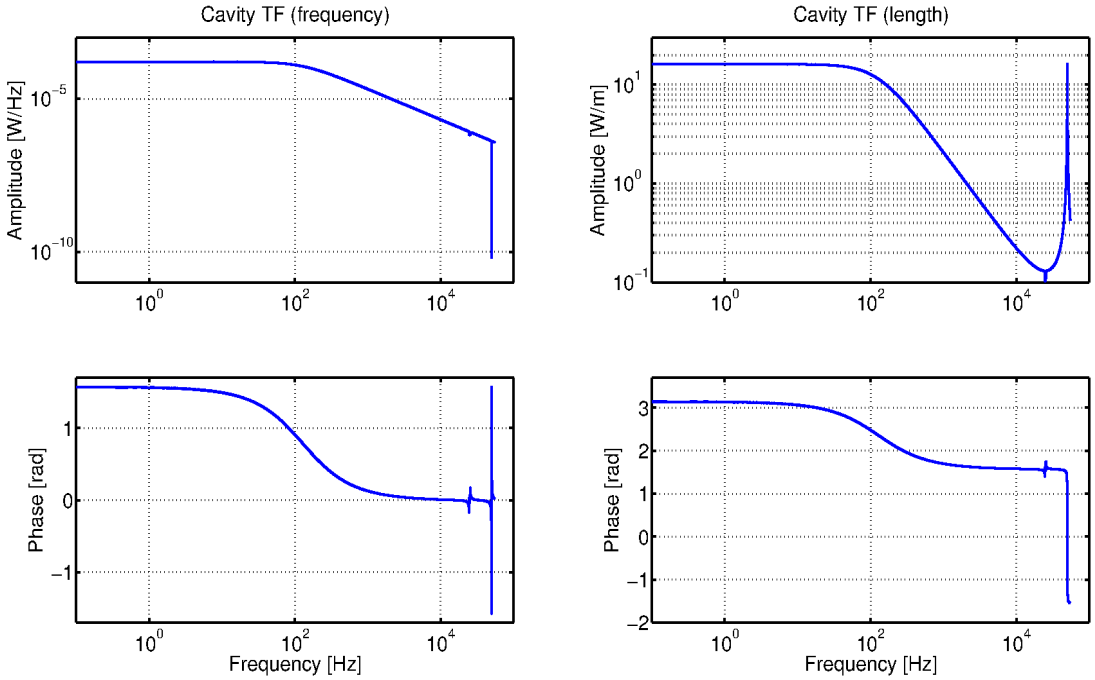

Figure 8: **Left picture:** Response of the arm cavity to a frequency variation. **Right picture:** Response of the arm cavity to a length variation.

The actuator transfer function is given by the manufacturer. In our case it is characterized by a simple pole at 30 kHz with a DC gain of 400 kHz/V. In practice this means that the actuator will not behave linearly above 30 kHz. The actuator could be chosen to have a higher bandwidth if needed. Notice that for what concerns the AOM it is able to follow up to the MHz region so it will not be a limiting factor.

Based on the shape of the TFs just presented the control filter can be designed. As a first approach it will satisfy: compensation of the pole of the cavity, high gain at low frequency where the seismic noise will be dominant, and an UGF high enough to control the frequency noise as much as possible. The limit of the UGF is imposed by the phase jump at the FSR, and in order to be safe we will not put the UGF higher than half a FSR, 25 kHz. The actuator bandwidth will not be a limiting factor in this case.
The filter shape, the OL tranfer function and the stability diagram of the system for the designed filter are shown in Figure 9. From the Open Loop it can be seen that the UGF of the system is ∼25 kHz. The Nichols plot of Figure 9 shows that the system is unconditionally stable which means that it has an infinite gain margin,

very convenient from an experimental point of view. Notice as well that the phase jump at 50 kHz can not be seen on this diagram as mentioned previously.

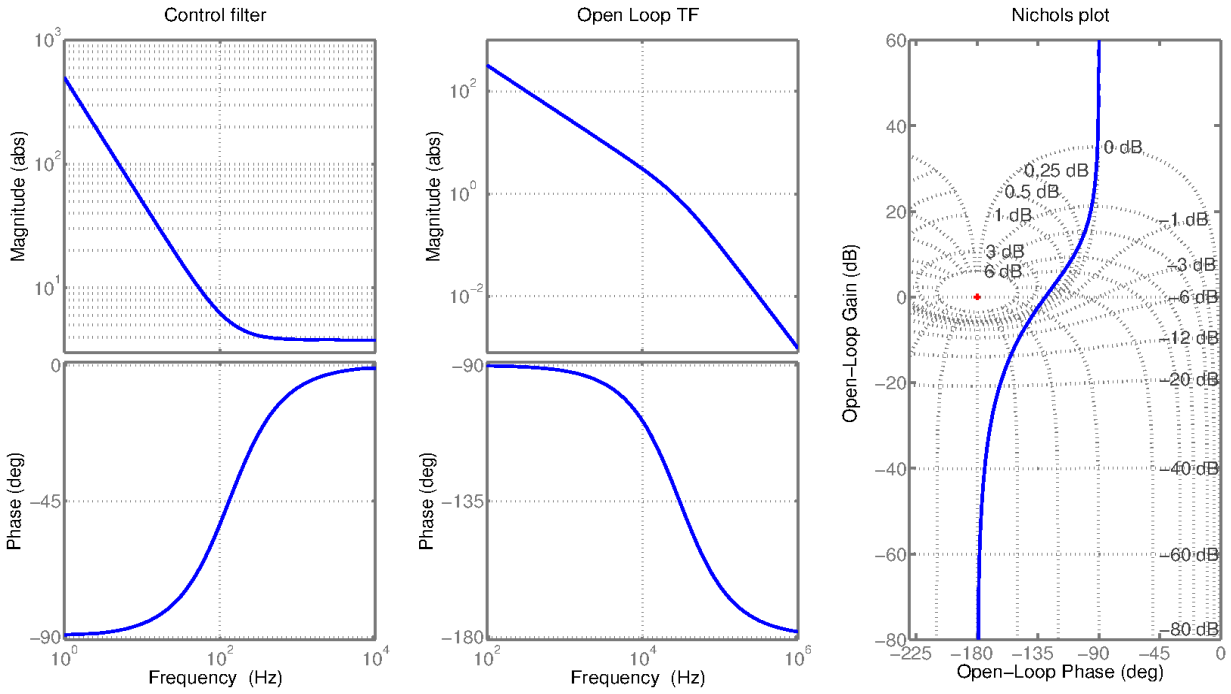

Figure 9: **Left picture:** TF of the control filter. **Central picture:** Open loop Transfer function of the system. **Right picture:** Nichols plot or stability plot of the system.

4.3 Relevant noises

The control strategy that is planned has been presented in the previous section. However there is another key element to take in account when evaluating the performance of the control system: the noise that brings the cavity out of resonance. Figure 9 shows two inputs: z_MIR, which refers to the **seismic noise** that causes the mirror motion; and f_FIB which corresponds to the **frequency noise** after the passage through the fibre. They are relevant because the study of the performance of the loop has sense only with respect to the perturbation that it tries to correct.

4.3.1 Cavity length variation

In order to have an idea of the longitudinal movement of the mirrors we need to take in account the top part of the suspensions. The seismic noise passes through all the filter chain down to the marionnetta, where there is no more active control engaged. This means that in practice the motion seen by the mirrors corresponds to the seismic noise filtered by the different control stages of the suspension top stage.
As this is quite a complex system, there is an easier way to measure experimentally the mirror motion: the correction of the longitudinal lock. It gives us the real movement of the mirrors due to the residual seismic noise that is not attenuated by the suspensions. The correction gives information up to the filter UGF which is 60 Hz, enough to cover the region where the remaining seismic noise is important. The shape of this noise is shown in Figure 10 being its rms ~ 1 μm.

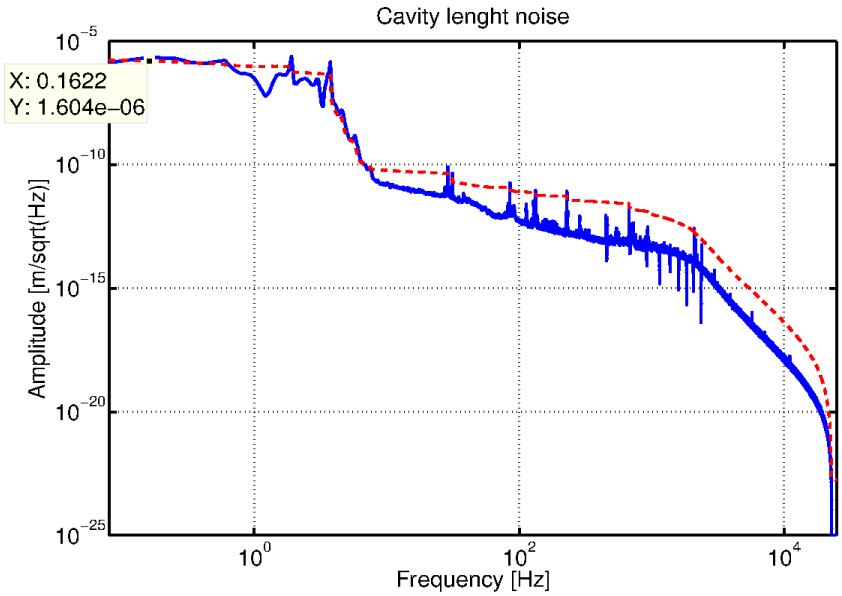

Figure 10: Cavity length movement spectrum as a blue continuous line with its integrated rms as the red dashed curve with a value of 1 μm.

4.3.2 Laser frequency variation

The frequency noise spectra at the exit of the fibre is more difficult to obtain. As presented on Section 3.2, we have measured the laser linewidth at the exit of the fibre although there is not a simple relationship that converts this information into a noise spectra. However, is we suppose that the environmental noise couples to the fibre as flicker frequency noise, a relationship between the noise level and the measured linewidth can be found in [16]. According to it, the power spectral density of the noise has the following shape:

$$S_{\delta\nu}(f) = a \cdot f^{-2} \tag{4.2}$$

where a can be calculated with the linewidth (FWHM) and the time of the measurement (T_0), solving the equations presented in [16]:

$$a = \frac{8 \cdot \ln(2) \cdot f_m^3}{\pi^2} \tag{4.3}$$

$$T_0 \cdot f_m^3 - f_m^2 = \left(\frac{FWHM \cdot \pi}{8 \cdot \ln(2)}\right)^2 \tag{4.4}$$

According to our measurement, the FWHM after the fibre is 740 Hz measured during $T_0 = 100$s. If the doubling of the frequency from 1064 nm to 532 nm is taken in account, the FWHM will become 1470 Hz. With these values we obtain a slope (a) = 3898.9 Hz^2/Hz. However, as we need an expression of the noise spectrum in $Hz/\sqrt{Hz}$, the final expression of our frequency noise at the exit of the fibre will be:

$$f_{FIB} = 62.5 \cdot f^{-1} \tag{4.5}$$

5 Longitudinal lock performance

Finally we have all the elements to evaluate the performance of the cavity lock. There are two stars on the schema that mark the points of the system which are relevant for the current study: the **residual frequency**

variation (yellow star), which provides information about the quality of the lock; and the **correction** needed to bring the system back to the working point (red star). The latter is important because the actuator has limited dynamics, and so it is necessary to check that the correction needed can be applied by the actuator.

5.1 Closed Loop equations

Their expressions can be obtained from solving the system equations in closed loop:

- **Residual frequency variation:**

$$f_{RES} = \frac{z_{ITF} \cdot CAV_z \cdot Filter \cdot Act - f_{FIB}}{1 - OL_{Las}} \tag{5.1}$$

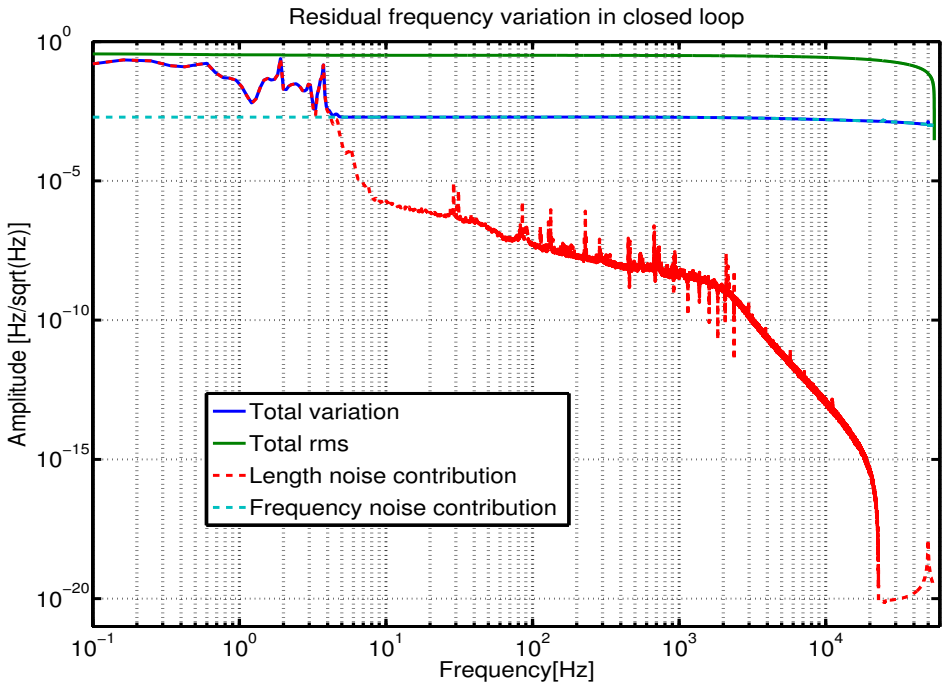

Figure 11: Spectrum of the residual frequency variation is the blue curve and its integrated rms is the green curve with a value of 0.35 Hz. The contribution from the length noise is the red dashed line and the one from the frequency noise is the blue dashed line.

Figure 11 shows the residual frequency variation as the continuous blue line, being the dashed lines the contributions coming from the mirror motion (red) and the frequency noise (light blue). The green line shows the rms of the residual frequency variation (0.35 Hz) which is dominated by the contribution of the frequency noise over the UGF where the feedback loop can not actuate. However it can be seen that the rms is largely lower than the requirements for power fluctuations under 10^{-1}. In particular it corresponds to power fluctuations under 10^{-3}.

- **Correction:**

$$CORR = z_{ITF} \cdot Filter \cdot CAV_z + f_{RES} \cdot Filter \cdot CAV_f \tag{5.2}$$

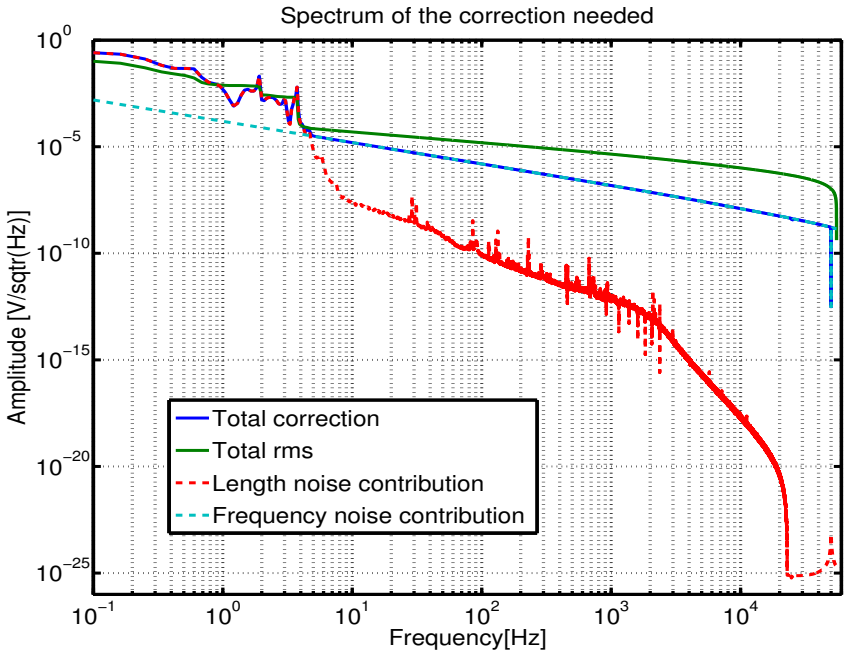

Figure 12: Spectrum of the correction needed in order to keep the cavity on resonance as the blue continuous line. Its rms is the green line with a value of 0.08 V. The contribution of the length noise is the red dashed line and the one of the frequency noise is the blue dashed line.

Finally Figure 12 shows the spectrum of the correction needed in order to reach the level of control just presented. Again, the continuous blue line represents the correction sent to the VCO with the dashed lines being the contributions from the mirror motion (red) and the frequency noise (light blue). The green line shows the rms of the correction (0.08 V) and it can be seen that is dominated by the longitudinal mirror displacement. It is indeed the gain at low frequency which demands more actuation dynamics, but still, the rms value remains significantly below the range that can be applied by the VCO.

6 Conclusion

After performing these measurements we can put an upper limit on the expected broadening of the laser linewidth caused by the propagation through a fibre of 3 km. The FWHM will be <1470 Hz for the green laser that will be injected into the arm cavity. The measurements performed on 20 m of fibre and the fact that the spectrum of the 6 km measurement is close to a Lorentzian suggests that the phase noise contribution to the broadening is significantly below this limit. With this noise level it has been proved that the laser can be locked to the arm cavity without the need of a phase noise cancellation system. Regarding the polar fluctuations it can be concluded that a power stabilization will be needed.

References

[1] N. Leroy; V. Loriette; B. Swinkels, 'Advanced Virgo Change request Auxiliary Lasers', Virgo note, 2014, VIR-0352A-13-v2. 2

[2] A. Staley et al., 'Achieving Resonance in the Advanced LIGO Gravitational-Wave Interferometer', Classical and Quantum Gravity, 24 (Vol. 31), 2014. 2

[3] Long-Sheng Ma; Peter Jungner; Jun Ye; John L. Hall, Accurate cancellation (to milliHertz levels) of optical phase noise due to vibration or insertion phase in fiber transmitted light. In Y. Shevy (Eds.), 'Laser Frequency Stabilization and Noise Reduction', SPIE Proceedings Vol. 2378, Apr. 1996. 2

[4] A. Aspect, 'Propietes statistiques de la lumiere laser', Ecole Polytechnique, Lecture. 5

[5] G. Pillant, J. Casanueva, E. Genin, A. Magazzu, Virgo logbook entry #33387, 15 March 2016. 4

[6] S. P. Singh; R. Gangwar; and N. Singh, 'Nonlinear scattering effects in optical fibers', Progress In Electromagnetics Research, PIER 74, 2007. 4

[7] S. Ten; M. Edwards, 'An introduction to the Fundamentals of PMD in fibers' (*White paper*), 2006. 4

[8] M. Mantovani; G. Vajente, 'Alignment accurary requirements for Advanced Virgo', Virgo note, 2010, VIR-247A-10. 6

[9] L. Pinard, 'Advanced Virgo End Mirror Characterization report- EM01', Virgo note, 2015, VIR-0269A-15. 6

[10] L. Pinard, 'Advanced Virgo Input Mirror Characterization report- IM02', Virgo note, 2014, VIR-0543A-14. 6

[11] L. Pinard, 'Advanced Virgo End Mirror Characterization report- EM03', Virgo note, 2015, VIR-0270A-15.

[12] L. Pinard, 'Advanced Virgo Input Mirror Characterization report- IM04', Virgo note, 2014, VIR-0544A-14. 6

[13] A. Freise, G. Heinzel, H. Luck, R. Schilling, B. Willke and K. Danzmann, 'Frequency domain interferometer simulation with higher-order spatial modes', Class. Quant. Grav. 21 (2004) S1067 [arXiv:gr-qc/0309012]. 6

[14] H. Heitmann, 'Laser frequency noise vs. PDH signal', ISC meeting presentation, October 2015, VIR-0543A-16. 8

[15] I. M. Littlewood, 'Spectral line broadening', California State University Stanislaus, 2016, Lecture. 8

[16] G. Di Domenico; S. Schilt; P. Thomann, 'Simple approach to the relation between laser frequency noise and laser line shape', Applied Optics, 49 (issue 25), 2010. 5

10